Model Predictive Control for Electromagnetic Launcher of UAV

Guanglei Xie, Jun Wu(✉), Yunzhou Zhang, and Yu Yang

School of Intelligent Science, National University of Defense Technology, Changsha 410073, Hunan, China
wujun2008@nudt.edu.cn

Abstract. Aim to improve the power density of the electromagnetic ejection system of UAV, the finite control set model prediction is adopted as the control strategy from the perspective of improving the efficiency. The semi-active control of hybrid energy storage system and the drive control of ejection motor are considered together. According to the different requirements of commutation and non-commutation, the finite control set of the electromagnetic ejection system is designed, control optimization is carried out from the system. Simulation results show that the proposed control strategy can effectively reduce thrust fluctuation, stabilize bus voltage, reduce switching loss and improve the efficiency of electromagnetic ejection system.

Keywords: UAV · Electromagnetic ejection · Power density · Model predictive control

1 Introduction

With the continuous development of artificial intelligence technology, UAV is more and more widely used in military and civil fields. As a launch mode with controllable speed in the whole process, electromagnetic ejection has the advantages of high reliability, strong concealment, easy maintenance and wide application range [1]. It is a research hotspot of UAV take-off mode at present. UAVs usually carry precision instruments, which requires the electromagnetic ejection system to have small overload impact, small thrust fluctuation and good controllability in the ejection process, so as to avoid damage to airborne equipment [2]. At the same time, UAVs of different types and weights should be ejected to the target speed according to different takeoff conditions, so as to fully reflect the advantages of electromagnetic ejection controllability [3].

With the development of high-speed microprocessor, model predictive control (MPC) is gradually applied to motor drive [4–6], power electronic converter [7, 8] and power system [9–11]. MPC does not rely on the accurate model of the controlled object and has the characteristics of "rolling optimization". At the same time, considering the state of the system in the future, it can optimize multiple control objectives. Therefore, it can achieve high-performance control effect for strong coupling, multi-objective and

X. Liang et al. (Eds.): *The proceedings of the 16th Annual Conference of China Electrotechnical Society*, LNEE 890, pp. 147–159, 2022.
https://doi.org/10.1007/978-981-19-1870-4_16

nonlinear motor system [12, 13]. Reference [14] proposes a finite set model predictive fault-tolerant control algorithm, which solves the problem of easy loss of excitation of permanent magnet synchronous motor under complex working conditions, and realizes the loss of excitation fault-tolerant control. Compared with the traditional PI control method, this method has stronger fault-tolerant ability and robustness; Reference [15] introduces high current constraint, switching state limit, maximum torque current ratio optimization (MTPA) and torque control into value function, which significantly improves the efficiency and robustness of permanent magnet synchronous motor control system while realizing MTPA control; Reference [16] proposed the control strategy of double vector MPC current loop, which acts two voltage vectors in one control cycle, increasing the selection range of voltage vector. The experiments show that the improved control algorithm effectively suppresses the torque fluctuation of permanent magnet synchronous motor, improves the response ability and tracking performance of current loop, and avoids the limitations of single vector MPC current loop; Document [17] analyzes the causes of commutation torque fluctuation of brushless motor in detail. By adding three states of convex, concave and constant non-commutation current in the commutation process, the stability of non-commutation current is effectively maintained and commutation torque fluctuation is reduced.

To sum up, MPC for permanent magnet synchronous motor mainly focuses on reducing torque ripple, improving efficiency and response speed by optimizing value function, expanding vector selection and increasing prediction cycle, so as to improve the performance of permanent magnet synchronous motor. The research on permanent magnet brushless DC motor system mainly focuses on the commutation stage. The commutation fluctuation is suppressed by increasing the control vector during the commutation stage, but the traditional PI control is still used in the non-commutation stage. Moreover, at present, all research is mainly focused on rotating motor, and the research on permanent magnet brushless linear DC motor is still blank. Different from the rotating motor, in the ejection stage, the permanent magnet brushless linear DC motor has been in the acceleration state. It has no steady state, only transient process. Therefore, the control performance of the ejection system has a great impact on the launch process of UAV. Therefore, this paper models the UAV electromagnetic ejection system as a whole, considers the energy control of the hybrid energy storage system and the drive control of the ejection motor, controls the ejection system as a whole, reduces the system loss, and improves the system efficiency.

2 Model Predictive Control Method for Electromagnetic Launcher of UAV

The electromagnetic ejection system of UAV consists of ejection motor, control system, drive system and energy storage system. The control idea of FCS-MPC is: since the switching states of power converters at the end of hybrid energy storage system and motor inverter are limited (DC/DC converter at the end of energy storage system includes 2 power converters, a total of 4 switching states; ejection motor inverter includes 6 power converters, a total of 8 switching States), the prediction model of hybrid energy storage system and ejection motor can be established, Calculate the predicted values of system

control variables corresponding to all switch states at the next time; Then, the value function is constructed to comprehensively evaluate the predicted value of the calculated system control variables, and the switching state corresponding to the minimum value function is selected; Finally, the switching state is applied to DC/DC converter and ejection motor inverter. Firstly, the prediction model of UAV electromagnetic ejection system needs to be established; Secondly, the objective function is designed for the object to be optimized. The model predictive control scheme of UAV electromagnetic ejection system is shown in Fig. 1. The outer loop of the system is speed loop and the inner loop is FCS-MPC current loop.

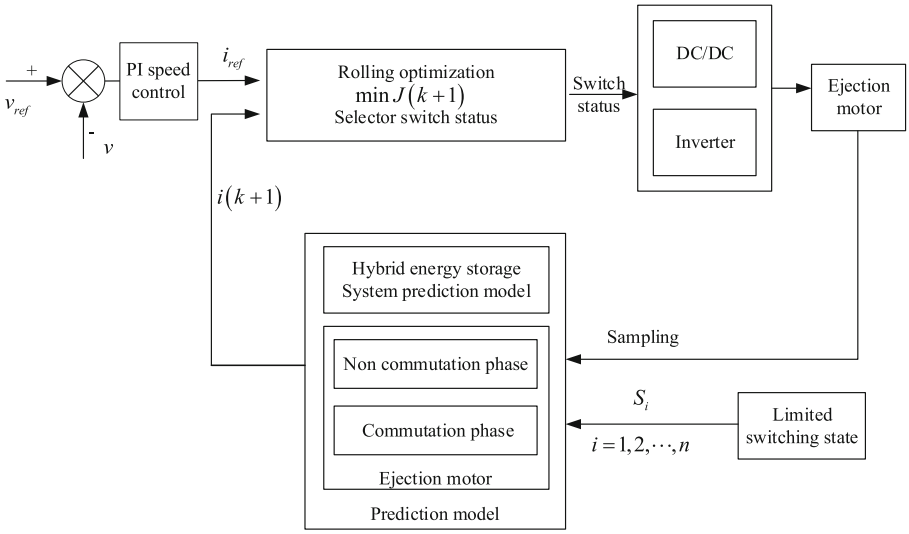

Fig. 1. Model predictive control scheme of UAV electromagnetic ejection system

The main circuit structure of UAV electromagnetic ejection system is shown in Fig. 2, which is mainly composed of hybrid energy storage system, inverter and ejection motor. In this paper, the hybrid energy storage system and ejection motor are predicted respectively.

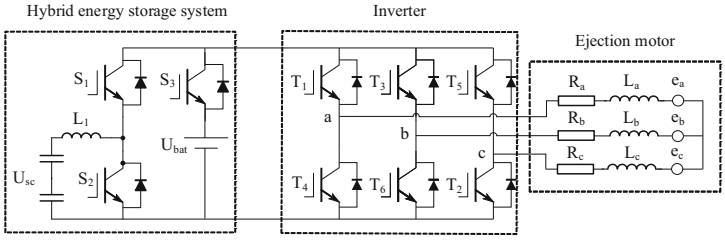

Fig. 2. Schematic diagram of main circuit structure of UAV electromagnetic ejection system

Current Prediction of Hybrid Energy Storage System. The structural block diagram of the hybrid energy storage system is shown in Fig. 3, which has four states and two working modes, as shown in Table 1. Among them, "1" is used when the power switch is on and "0" is used when it is off.

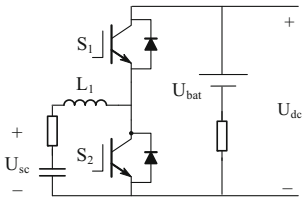

Fig. 3. Structure block diagram of hybrid energy storage system

Table 1. Working mode of hybrid energy storage system

Mode	States	S1	S2
Boost	1	0	1
Boost	2	0	0
Buck	3	1	0
Buck	4	0	0

The four working states are discretized by the first-order Euler method, and the predicted current of the hybrid energy storage system at time is obtained as follows:

$$
\begin{aligned}
i_{sc\_1}(k+1) &= \frac{T_s}{L}U_{sc}(k) + i_{sc}(k) \\
i_{sc\_2}(k+1) &= \frac{T_s}{L}[U_{sc}(k) - U_{dc}(k)] + i_{sc}(k) \\
i_{sc\_3}(k+1) &= \frac{T_s}{L}[U_{dc}(k) - U_{sc}(k)] + i_{sc}(k) \\
i_{sc\_4}(k+1) &= -\frac{T_s}{L}U_{sc}(k) + i_{sc}(k)
\end{aligned} \tag{1}
$$

Ejection Motor Current Prediction. The three-phase windings of the ejection motor are star connected, the motor is driven by square wave current, and the two-way conduction mode is adopted during operation. The simplified equivalent circuit is shown in Fig. 4, where T1–T6 is IGBT power device, U_DC is the bus voltage and N is the neutral point of the motor.

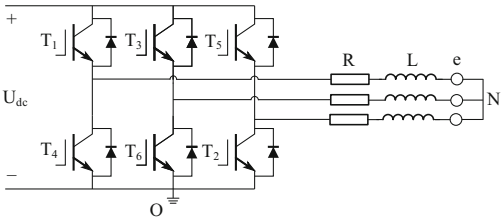

Fig. 4. Simplified equivalent circuit model of ejection motor

The voltage balance equation of the ejection motor is

$$\begin{bmatrix} u_{ao} \\ u_{bo} \\ u_{co} \end{bmatrix} = \begin{bmatrix} R & 0 & 0 \\ 0 & R & 0 \\ 0 & 0 & R \end{bmatrix} \begin{bmatrix} i_a \\ i_b \\ i_c \end{bmatrix} + \begin{bmatrix} L & 0 & 0 \\ 0 & L & 0 \\ 0 & 0 & L \end{bmatrix} \frac{d}{dt} \begin{bmatrix} i_a \\ i_b \\ i_c \end{bmatrix} + \begin{bmatrix} e_a \\ e_b \\ e_c \end{bmatrix} + \begin{bmatrix} u_{no} \\ u_{no} \\ u_{no} \end{bmatrix} \tag{2}$$

Where u_{ao}, u_{bo}, u_{co} is the voltage of the three-phase winding end of the ejection motor to the ground; i_a, i_b, i_c is the three-phase current of the ejection motor; e_a, e_b, e_c is the three-phase back EMF of the ejection motor; R is the equivalent resistance of each phase winding of the ejection motor; L is the equivalent inductance of each phase winding of the ejection motor; u_{no} is the neutral point to ground voltage of the ejection motor.

The ejection motor adopts the conduction control mode of three-phase and six states, which is divided into two situations.

Current Prediction in Normal Two-Phase Conduction Stage. In an electrical cycle, the ejection motor corresponds to six two-phase conduction modes, and the conduction condition and optional switching state of the corresponding power switch are shown in Table 2.

Table 2. Optional switch States in non-commutation mode

Non-commutation mode	Turn on the power switch tube	States 1	States 2
I	T_1T_2	110000	100000
II	T_3T_2	011000	001000
III	T_3T_4	001100	001000
IV	T_5T_4	000110	000010
V	T_5T_6	000011	000010
VI	T_1T_6	100001	100000

Since the processes of six two-phase conduction modes are consistent, mode I is taken as an example. As shown in Fig. 5, it is the schematic diagram of switching state 1 in the two-phase conduction stage. At this time, the power switch tube T1T2 is on.

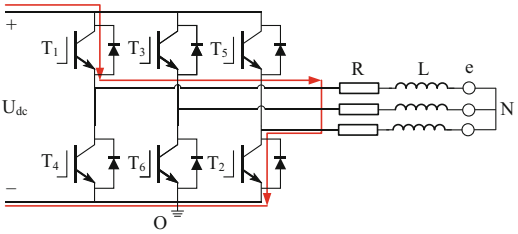

Fig. 5. Schematic diagram of switch state 1 in two-phase conduction stage

The voltage equation of the ejection motor is

$$\begin{cases} u_{ao} = i_a R + L_s \frac{di_a}{dt} + e_a + u_{no} \\ u_{co} = i_c R + L_s \frac{di_c}{dt} + e_c + u_{no} \\ i_a = -i_c \\ u_{ao} - u_{co} = 2i_a R + 2L_s \frac{di_a}{dt} + e_a - e_c = U_{dc} \end{cases} \tag{3}$$

By discretization, the predicted current of phase a at K + 1 is

$$i_a(k+1) = i_a(k) + \frac{T_s}{2L_s}[U_{dc}(k) - (e_a(k) - e_c(k)) - 2i_a(k)R] \tag{4}$$

As shown in Fig. 6, it is the schematic diagram of switching state 2 in the two-phase conduction stage.

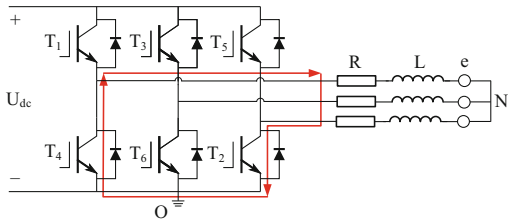

Fig. 6. Schematic diagram of switch state 2 in two-phase conduction stage

By discretization, the predicted current of phase a at K + 1 is

$$i_a(k+1) = i_a(k) + \frac{T_s}{2L_s}[-(e_a(k) - e_c(k)) - 2i_a(k)R] \tag{5}$$

Current Prediction Model in Commutation Stage. The optional switch states under different commutation modes are shown in Table 3. There are four circuit conduction states under each commutation mode.

Table 3. Optional switch states in different commutation modes

Non-commutation mode	States 1	States 2	States 3	States 4
I	001000	011000	101000	111000
II	000100	001100	010100	011100
III	000010	000110	001010	001110
IV	000001	000011	000101	000111
V	100000	100001	100010	100011
VI	010000	110000	010001	110001

Taking commutation mode I as an example, at this time, phase C is non-commutation phase, phase A is off phase and phase B is on phase, then

$$\begin{aligned} u_{ao} - u_{bo} &= (-2i_b - i_c)R + L_s(-2\frac{di_b}{dt} - \frac{di_c}{dt}) + (e_a - e_b) \\ u_{bo} - u_{co} &= (i_b - i_c)R + L_s(\frac{di_b}{dt} - \frac{di_c}{dt}) + (e_b - e_c) \\ u_{ao} + u_{bo} - 2u_{co} &= -3Ri_c - 3L_s\frac{di_c}{dt} + (e_a + e_b - 2e_c) \end{aligned} \tag{6}$$

By discretization, the predicted current of phase C at K + 1 is

$$\begin{aligned} (1 + \frac{RT_s}{L_s})i_c(k+1) - i_c(k) = \frac{T_s}{3L_s}[(e_a(k) + e_b(k) - 2e_c(k)) \\ - (u_{ao}(k) + u_{bo}(k) - 2u_{co}(k))] \end{aligned} \tag{7}$$

Make

$$\begin{aligned} e(k) &= e_a(k) + e_b(k) - 2e_c(k) \\ u(k) &= u_{ao}(k) + u_{bo}(k) - 2u_{co}(k) \end{aligned} \tag{8}$$

Can be reduced to

$$(1 + \frac{RT_s}{L_s})i_c(k+1) - i_c(k) = \frac{T_s}{3L_s}[e(k) - u(k)] \tag{9}$$

Then at K + 1, the predicted current of phase C is

$$i_c(k+1) = \frac{1}{1 + \frac{RT_s}{L_s}}\left\{\frac{T_s}{3L_s}[e(k) - u(k)] + i_c(k)\right\} \tag{10}$$

Similarly, the terminal voltages corresponding to different switching states under different commutation modes can be obtained, as shown in Table 4 (UDC is represented by 1). The predicted current value of the non-commutating phase at K + 1 can be calculated.

Table 4. Terminal voltage corresponding to different switching states

Commutation mode	I	II	III	IV	V	VI
1	011	001	101	100	110	010
2	010	011	001	101	100	110
3	111	000	111	000	111	000
4	110	010	011	001	101	100

Model Switching Algorithm of Ejection Motor

Table 5. Ejection motor commutation time detection table

Commutation mode	Non-commutation	Start time of commutation	End time of commutation	Judgment conditions
I	C	H2↑	ia = 0	H2 = 1, ia > 0
II	B	H1↓	ic = 0	H1 = 0, ic < 0
III	A	H3↑	ib = 0	H3 = 1, ib > 0
IV	C	H2↓	ia = 0	H2 = 0, ia < 0
V	B	H1↑	ic = 0	H1 = 1, ic > 0
VI	A	H3↓	ib = 0	H3 = 0, ib < 0

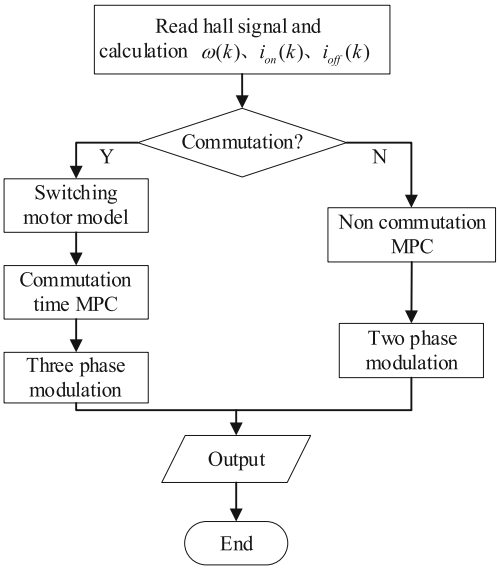

Fig. 7. Ejection motor prediction model switching process

The commutation time of the ejection motor is shown in Table 5. When the rising edge and falling edge signals of the hall signal are detected, the ejection motor enters the commutation stage. The specific switching process is shown in Fig. 7.

Rolling Optimization. The optimization objectives of FCS-MPC in this paper include the following points:

The Thrust Fluctuation is Small. The ejection motor described in this paper is a permanent magnet brushless DC linear motor, which will produce large thrust fluctuation during commutation. It can be seen from literature [18] that the thrust fluctuation is

$$\Delta F = \frac{(F_{\min} - F_{avg})}{F_{avg}} = \frac{U_{dc} - 4E - 3Ri}{U_{dc} + 2E + 3Ri} \tag{11}$$

Therefore, the optimization objective is

$$\left| i_{non}(k+1) - i_{non\_ref} \right| \tag{12}$$

Where $i_{non}(k+1)$ is the predicted current at the time K + 1,i_{non_ref} is the calculated reference current.

Less Switching Times of Power Devices. On the premise of determining the structure of UAV electromagnetic ejection system, the system loss can be reduced by reducing the switching times of power converter, so as to improve the efficiency of electromagnetic ejection system [19], which is

$$\begin{aligned} S_{switch}(k+1) = {} & |S_a(k+1) - S_a(k)| + |S_b(k+1) - S_b(k)| \\ & + |S_c(k+1) - S_c(k)| + |S_{dcdc}(k+1) - S_{dcdc}(k)| \end{aligned} \tag{13}$$

Where the first three items are the switching action times of phase a, b and c power devices of inverter respectively; $|S_{dcdc}(k+1) - S_{dcdc}(k)|$ is the switching action times of DC/DC converter.

Super Capacitor Current Tracking Error is Small. That is, the discharge current of super capacitor is required to track the calculated reference current in time. The optimization objectives is

$$\left| i_{sc}(k+1) - i_{sc\_ref} \right| \tag{14}$$

Where $i_{sc}(k+1)$ is the predicted current of supercapacitor at time $k+1$; i_{sc_ref} is the supercapacitor reference current calculated by power distribution.

Therefore, in the UAV electromagnetic ejection system, in order to improve the power density, from the perspective of improving efficiency, in order to reduce the thrust fluctuation, the switching times of power devices and the battery discharge current fluctuation, the multi-objective value function can be formulated as follows

$$\min J(k+1) = \alpha\left|i_{non}(k+1) - i_{non\_ref}\right| + \beta S_{switch}(k+1) + \lambda\left|i_{sc}(k+1) - i_{sc\_ref}\right| \tag{15}$$

Where α, β, λ are the weight coefficients corresponding to the control target respectively.

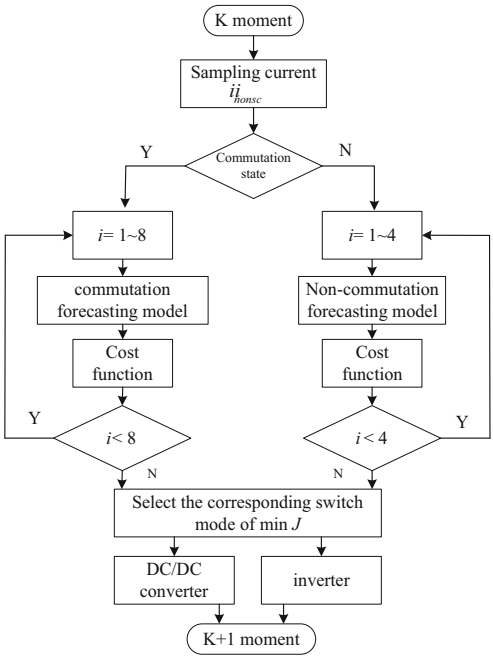

Fig. 8. FCS-MPC control process of UAV electromagnetic ejection system

In this paper, the FCS-MPC control strategy adopts the single-step prediction method, and the prediction step and control step are 1. Therefore, in the prediction process, the "exhaustive method" can be used to solve the optimal switching sequence of the system. The FCS-MPC control process of UAV electromagnetic ejection system is shown in Fig. 8.

3 Simulation Analysis

In order to verify the effectiveness of the FCS-MPC control algorithm proposed in this paper, the simulation model of UAV electromagnetic ejection system is built in

Matlab/Simulink environment for analysis, and the MPC algorithm is compared with the traditional PI control algorithm. The working voltage of UAV electromagnetic catapult is 340 V, and the parameters used in simulation are shown in Table 6.

Table 6. Simulation parameters of UAV electromagnetic ejection system

Classes	Parameter
Nominal voltage of lithium battery/V	340
Nominal capacity of lithium battery/Ah	200
Nominal voltage of supercapacitor/V	288
Nominal capacity of supercapacitor/F	45
Phase inductance of ejection motor/mH	0.085
Phase resistance of ejection motor/Ω	2.875

The simulation results are shown in Fig. 9.

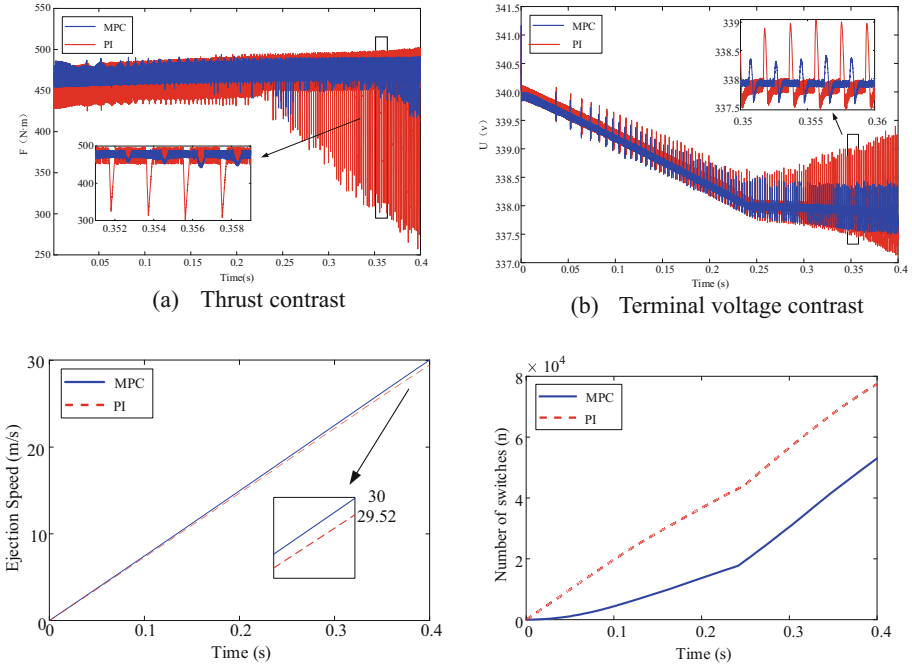

(a) Thrust contrast

(b) Terminal voltage contrast

(c) Switch frequency comparison

(d) The ejection velocity contrast

Fig. 9. Comparison of FCS-MPC and PI control strategy simulation results

Figure 9(a) shows the thrust comparison between FCS-MPC control strategy and PI control strategy. It can be seen that in the early stage of ejection, the thrust fluctuation

of FCS-MPC control strategy is 3.2%, while that of PI control strategy is 5.8%. In the later stage of ejection, with the increase of the mover speed, the back EMF of the motor is satisfied $U_{dc} - 4E < 3Ri$, and PI control can not suppress the thrust fluctuation. At this time, the maximum thrust fluctuation reaches 45.3%, resulting in the decrease of effective thrust. The FCS-MPC control strategy can effectively maintain the stability of non-commutation current, suppress the thrust fluctuation within 13.7% and effectively reduce the thrust fluctuation by increasing the vector selection of ejection single machine during commutation.

Figure 9(b) shows the terminal voltage comparison between FCS-MPC control strategy and PI control. It can be seen that in the early stage of ejection, the required power of the motor is less than that provided by the battery. At this time, all power is provided by the lithium battery. The current of the lithium battery increases with the increase of ejection speed, and the terminal voltage decreases with the increase of battery output current. When the required power of the ejection motor is greater than the maximum power provided by the battery, the insufficient power is supplemented by the super capacitor. At this time, the lithium battery maintains the maximum discharge current and the terminal voltage does not drop. By adopting FCS-MPC strategy, the fluctuation of terminal voltage in the later stage of ejection can be reduced from 1.5 V to 0.5 V, which effectively protects the battery.

Figure 9(c) shows the comparison of switching times of power devices controlled by FCS-MPC and PI. By introducing a new switching vector in the motor commutation process, the switching times can be effectively reduced. In one ejection process, the switching times can be effectively reduced by 31%.

Figure 9(d) shows the ejection speed comparison between FCS-MPC control strategy and PI control. It can be seen that in the same ejection time, the ejection end speed of FCS-MPC is greater than that controlled by PI, which shows that FCS-MPC algorithm has higher efficiency and can indirectly improve the system power density.

4 Conclusion

In order to reduce the loss and improve the efficiency of UAV electromagnetic ejection system, an FCS-MPC method is proposed to manage the energy from the whole system, and optimize the motor thrust fluctuation, bus voltage fluctuation and power switching loss. Compared with traditional PI control, FCS-MPC method can optimize multiple objectives at the same time, which is embodied in:

(1) The thrust fluctuation during commutation is reduced from 45.3% to 13.7%, and the thrust fluctuation during non-commutation is reduced from 5.8% to 3.2%;
(2) The fluctuation of bus voltage is reduced from 1.5 V to 0.5 V, which improves the stability of lithium battery terminal voltage;
(3) In one ejection process, the switching times of power devices are effectively reduced by 31% and the switching loss is reduced;
(4) At the same time, FCS-MPC has higher ejection terminal velocity, indicating that FCS-MPC scheme can effectively improve system efficiency.

References

1. Wang, H., Yang, M.: Development status and trend of U.S. UAV. Flying Missile **2**, 46–50 (2020). (in Chinese)
2. Wang, X., Wu, J., Meng, Q.: Design of a continuous electromagnetic ejection system for UAV. Fire Command Control **46**(4), 7 (2021). (in Chinese)
3. Du, P., Lu, J., Li, X., et al.: Interior ballistic characteristics of electromagnetic rail launcher considering the dynamic characteristics of real launcher. IEEE Trans. Ind. Electron. **68**(7), 6087–6096 (2021)
4. Ahmed, A.A., Koh, B.K., Lee, Y.I.: A comparison of finite control set and continuous control set model predictive control schemes for speed control of induction motors. IEEE Trans. Ind. Inform. **14**(4), 1334–1346 (2018)
5. Li, X., Wang, Y., Guo, X., Cui, X., Zhang, S., Li, Y.: An improved model-free current predictive control method for SPMSM drives. IEEE Access **9**, 134672–134681 (2021)
6. Mousavi, M.S., Davari, S.A., Nekoukar, V., Garcia, C., Rodriguez, J.: Finite-set model predictive current control of induction motors by direct use of total disturbance. IEEE Access **9**, 107779–107790 (2021)
7. Wang, M., Shi, Y., Shen, M., et al.: Model voltage predictive control of three-phase voltage source rectifier. J. Electrotech. Technol. **30**(16), 49–55 (2015). (in Chinese)
8. Rodríguez, J., Heydari, R., Rafiee, Z., Young, H.A., Flores-Bahamonde, F., Shahparasti, M.: Model-free predictive current control of a voltage source inverter. IEEE Access **8**, 211104–211114 (2020)
9. Rodriguez, J., Garcia, C., Mora, A., et al.: Latest advances of model predictive control in electrical drives. Part I: basic concepts and advanced strategies. IEEE Trans. Power Electron. **37**, 3927–3942 (2022)
10. Rodriguez, J., Garcia, C., Mora, A., et al.: Latest advances of model predictive control in electrical drives. Part ii: applications and benchmarking with classical control methods. IEEE Trans. Power Electron. **37**, 5047–5061 (2021)
11. Hu, J., Shan, Y., Guerrero, J.M., et al.: Model predictive control of microgrids–an overview. Renew. Sustain. Energy Rev. **136**, 110422 (2021)
12. Rodriguez, J., Cortes, P.: Predictive Control of Power Converters and Electrical Drives (2012)
13. Xi, Y.: Predictive Control. National Defense Industry Press, Beijing (2013). (in Chinese)
14. Zhao, K., Chen, Y., Zhang, C., et al.: Finite set model predictive fault-tolerant control of PMSM loss-of-excitation fault. J. Electr. Meas. Instrum. **33**(7), 84–92 (2019). (in Chinese)
15. Liu, X., Liu, W.: Based on the maximum torque current ratio control of permanent magnet synchronous motor. J. Model Predictive Control Mot. Control Appl. **4** (2017). (in Chinese)
16. Lin, J., Xie, G., Wan, Q., et al.: Improved double vector MPC current control of permanent magnet synchronous linear motor. Micro-spec. Mot. **47**(8), 48–53 (2019). (in Chinese)
17. Zhang, Y., Cui, W., Liao, J.: Brushless DC motor torque ripple suppression method based on model predictive control. Micro-spec. Mot. **43**(2), 58–61 (2015). (in Chinese)
18. Lu, S., Zhao, H., Wu, J.: Fluctuation analysis of commutation thrust of brushless DC linear motor for ejection. Micro Mot. **38**(6), 10–12 (2010). (in Chinese)
19. Luo, R., He, Y., Chen, H., et al.: SVPWM strategy of neutral point potential balance and low switching loss of three-level converter. J. Electrotech. Technol. **33**(14), 3245–3254 (2018). (in Chinese)